Article ID: 1000-7032(2013)10-1351-07

A Plasmonic Laser Source Based On Bragg Reflection Waveguide

CHEN Yong-yi[1,2], QIN Li[1*], TONG Cun-zhu[1], WANG Li-jun[1], NING Yong-qiang[1], LIU Yun[1], WANG Li-jie[1,2], ZHANG Jin-long[1], SHAN Xiao-nan[1]

(1. *State Key laboratory of Luminescence and Applications, Changchun Institute of Optics, Fine Mechanics and Physics, Chinese Academy of Sciences, Changchun* 130033, *China*;
2. *University of Chinese Academy of Sciences, Beijing* 100049, *China*)
* *Corresponding Author, E-mail: qinl@ciomp.ac.cn*

Abstract: We designed a new type of plasmonic laser source based on the Bragg reflection waveguide. This laser source is simple in structure and convenient for integration. It works under room temperature electrical pumping condition and outputs plasmonic laser with more than milliwatt power, which is much larger than those demonstrated plasmonic laser sources with power of nano-watt scale. The proposed laser works at 808 nm. The tilted light beam offered by Bragg reflection waveguide directly couples into surface plasmon polaritons in our quasi-Otto configuration.

Key words: semiconductor lasers; Bragg reflection waveguide; plasmonics
CLC number: O469 **Document code**: A **DOI**: 10.3788/fgxb20133410.1351

一种基于布拉格反射波导的表面等离子体激光光源

陈泳屹[1,2], 秦 莉[1*], 佟存柱[1], 王立军[1], 宁永强[1], 刘 云[1], 汪丽杰[1,2], 张金龙[1], 单肖楠[1]

(1. 发光学及应用国家重点实验室 中国科学院长春光学精密机械与物理研究所, 吉林 长春 130033;
2. 中国科学院大学, 北京 100049)

摘要: 设计了一种基于布拉格反射波导的新型表面等离子体激光光源。这种光源结构简单,便于集成,可以在室温电泵浦的条件下工作,同时可以输出约毫瓦量级的表面等离子激光,相比于文献报道中纳米尺度的纳瓦级表面等离子体激光光源要高很多。该表面等离子体激光光源发射波长为808 nm,布拉格反射波导所提供的倾斜激光光线在我们设计的准Otto模型中可以直接耦合成为表面等离子体。

关 键 词: 半导体激光; 布拉格反射; 表面等离子体

收稿日期: 2013-05-01; **修订日期**: 2013-07-03
基金项目: 国家自然科学基金重点项目(61234004); 国家自然科学基金面上项目(61176045); 国家自然科学青年基金(61106068)资助项目
作者简介: 陈泳屹(1986-), 男, 吉林长春人, 主要从事表面等离子体和半导体激光器方面的研究。
E-mail: cyy2283@126.com, Tel: (0431)86176335

1 Introduction

Plasmon lasers[1-4] which can supply laser sources below diffraction have been intensely studied recently. These lasers have been applied in many fields, such as on-chip optical interconnects, dense photonic circuits, biological or chemical sensors and data recording sources[5-11]. On one hand, many plasmonic lasers[1-4] have the advantages of nano-scale cavity, small optical mode size, high modal gain and easy in integration, but they suffer the large Ohmic losses due to the introduced metal structures. Moreover, electrically pumped plasmon lasers are even more difficult to fabricate because of the delicate accuracy in the nano scale and the complicated handcraft. These drawbacks limit their applications. This type of laser is usually hard to work at room temperature (RT) and the emission power is usually very low (~nW) because of the small cavity[1-2]. On the other hand, in many cases we need high power plasmonic laser sources, which can be built in the photonic chips and circuits, such as nano optical lithography, biological or chemical sensing, data recording, *etc.* In these situations what we need are not the plasmonic laser elements in nanoscale, but the plasmonic laser sources which are strong enough and easy for integration, meanwhile working at RT and under electrically pumping condition. Surface plasmon polaritons (SPPs) usually need pumping sources, prisms or gratings *etc.*[12-14], which make the total structure too large and difficult for integrations.

In this paper, we present a new type of plasmonic laser source based on Bragg reflection waveguide (BRW). This plasmonic laser source works at 808 nm, at RT electrical pumping condition. A specific Ⅲ-Ⅳ GaAs substrate side emitting semiconductor laser structure was used to assure the laser source work under electrical pumping condition and at RT, as well as easy for integration and direct application. SiO_2 and gold layers were deposited consequently on one cleavage facet of the semiconductor part. The BRW offers titled optical beams in the optical cavity, forming a quasi-Otto configuration together with the SiO_2 and gold layer.

2 Structure of The Plasmonic Laser Source

Fig. 1 showed the schematic diagram of the designed plasmonic laser source, which was made up of the semiconductor region and plasmonic region. The semiconductor region consisted of the BRW, adapting waveguide layer (AWL), gain medium quantum well (QW) and top total internal reflection (TIR) waveguide. The plasmonic region located at cleavage facet of the semiconductor part, which consists of a layer of SiO_2 and a layer of gold. The AWL, SiO_2 and Au act as a quasi-Otto configuration, meanwhile, the AWL is designed for meeting the effective index of the cavity conditions and the Otto configuration conditions. The BRW supplies beams with specific angle θ directly couples into SPPs that travels along the boundary of SiO_2 and Au. The plasmonic laser goes both up and down along metal in y axis. The detailed structure parameters, such as the material and thickness, were decided by the following theoretical calculation.

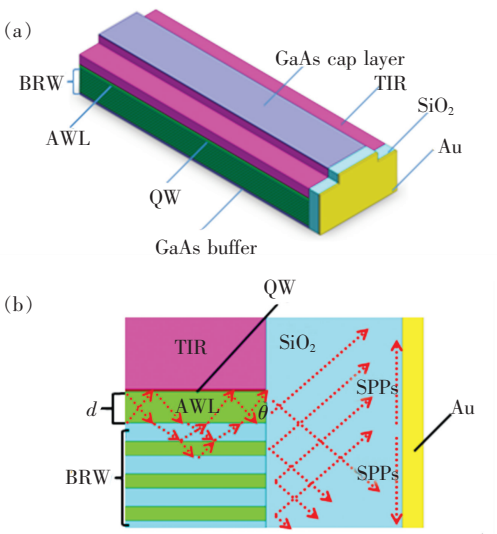

Fig. 1 Structure of the plasmonic laser source. (a) 3D figure of the plasmonic laser source. (b) 2D detail of the specific region. The doted lines demonstrate the optical beam propagation directions.

3 The Theoretical Design of The Plasmonic Laser Source

3.1 Standard Otto Configuration

First, the standard Otto configuration is considered.

Gold has a complex permittivity, which can be expressed as $\varepsilon_{Au} = \varepsilon_1 + i\varepsilon_2$. The permittivity of SiO_2 is ε_{SiO_2}. According to the plasmonic theory[15], the SPPs travelling along the boundary of SiO_2 and Au have the wave vector:

$$k_{SPP} = k_0 \sqrt{\frac{\varepsilon_1 \varepsilon_{SiO_2}}{\varepsilon_1 + \varepsilon_{SiO_2}}}, \quad (1)$$

where k_0 is the wave vector in vacuum. The coupling angle θ from the semiconductor to plasmonic region must obey[12]:

$$k_{SPP} = k_0 n_s \cos\theta, \quad (2)$$

where n_s is the material index of the AWL. In this paper, $Al_{0.3}Ga_{0.7}As$ was selected as the AWL, whose refractive index is about 3.437 at 808 nm. The corresponding refractive index of Au and SiO_2 at 808 nm are 0.1833 − 5.2133i and 1.450 2, respectively. Because the permittivity ε and refractive index obey

$$\varepsilon = (n - ik)^2, \quad (3)$$

where n and k are the real and imaginary part of the material respectively. A 2D finite-difference time-domain method (FDTD method) simulation was carried out using Lumerical FDTD Solutions software to disclose the influence of θ on total reflection. Then the values of k_{SPP} and θ could be obtained. Fig. 2 gave the relationship between the reflection of standard Otto configuration and the incident angle $\varphi = 90° - \theta$. The thickness of SiO_2 was set to be 600 nm. We had a minimal incident angle around 26.03°, which was quite near the analytical solution 26.05° solved by equations (1) ~ (3). The minimal reflection meant the highest coupling efficiency.

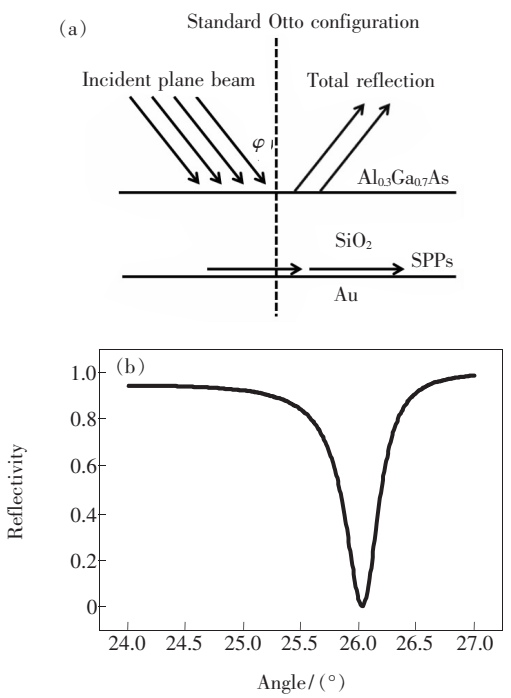

Fig. 2　FDTD simulation results for standard Otto configuration. (a) Demonstration of a standard Otto configuration. (b) Relationship between the incident angle $\varphi = 90° - \theta$ of standard Otto configuration and total reflection solved by FDTD method.

3.2　Design of The Plasmonic Laser Source

In our design, the optical source was supplied by the semiconductor waveguide optical mode instead of plane wave used in the 2D FDTD simulation above. In order to maximize the effective coupling from photons to SPPs, the mode effective index n_{eff}, semiconductor material index n_s and SPP wave vector k_{SPP} must obey:

$$k_{SPP}^2 + k_0^2 n_{eff}^2 = k_0^2 n_s^2, \quad (4)$$

so n_{eff} had an analytical solution at 3.089 for the selected AWL as $Al_{0.3}Ga_{0.7}As$. The Bragg reflectors are quarter-wavelength reflectors, so the thickness of each Bragg reflector layer's thickness obeys[16]:

$$k_1 a = k_2 b = \frac{\pi}{2}, \quad (5)$$

where a and b are the thickness of Bragg reflector layers, k_1 and k_2 are the corresponding wave vector which obey:

$$k_i^2 + k_{eff}^2 = k_0^2 n_i^2 \ (i = 1, 2), \quad (6)$$

n_i is the corresponding material refractive index, and $k_{eff} = k_0 n_{eff}$. More power was supposed to be coupled into SPPs, so the higher index material for the BRW was also selected as $Al_{0.3}Ga_{0.7}As$, the corresponding thickness was 138 nm. The low refractive index material was selected as $Al_{0.5}Ga_{0.5}As$, with a material index 3.300, and the corresponding thickness was 173 nm. The reflective layer on top of the QW must act as TIR layer, so its refractive index must be smaller than effective index 3.089. In this case, the 2 μm $Al_{0.9}Ga_{0.1}As$ was capable to be the TIR layer, which had a material index at 3.06.

To obtain the thickness of AWL, the dependence of mode effective index on the AWL thickness was calculated by using MODE Solutions software.

The thickness of AWL d adjacent to the QW was adjusted, to ensure the total effective index as designed. Notice that mode effective index smaller than $Al_{0.9}Ga_{0.1}As$ didn't have physical meanings. Fig. 3 demonstrates the relationship of d and n_{eff}. The material index for $GaAs_{0.86}P_{0.14}$ QW was 3.640, and for barrier $Al_{0.4}Ga_{0.6}As$ was 3.366. the thickness d was 267 nm with a mode effective index of 3.089.

The thickness of the SiO_2 varied from 300 nm to 3 000 nm in our calculation. The gold layer was 100 nm thick, thick enough to annihilate transmission. The ridge of the semiconductor in this article was supposed to be 1 μm in depth and 5 μm in width. Suppose the whole length of the semiconductor lasers was 0.5 mm. The detailed structure of the semiconductor region is shown in Fig. 4.

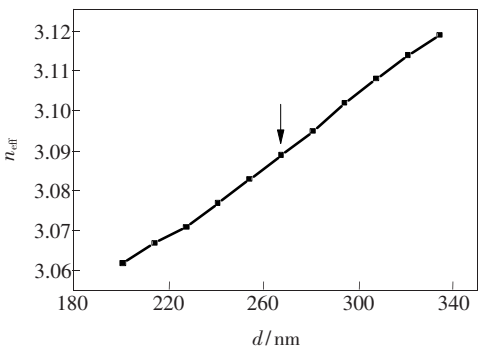

Fig. 3 Relationship between d and mode effective index. For designed effective index at 3.088, the thickness of d is selected at 267 nm.

100 nm p^+ GaAs cap layer	
2 000 nm p^- $Al_{0.9}Ga_{0.1}As$	
QW	10 nm $Al_{0.4}Ga_{0.6}As$
	11 nm $GaAs_{0.86}P_{0.14}$
	10 nm $Al_{0.4}Ga_{0.6}As$
267 nm n^- $Al_{0.3}Ga_{0.7}As$	
9×	173 nm n^- $Al_{0.5}Ga_{0.5}As$
	138 nm n^- $Al_{0.3}Ga_{0.7}As$
300 nm n^+ GaAs buffer	
n^+ GaAs substrate	

Fig. 4 The detailed structure of semiconductor region in the 808 nm plasmonic laser source

4 Analysis of the Designed Plasmonic Laser Source

For the designed plasmonic lasers, lasing or not was determined by the threshold gain and loss. Numerical simulations were carried out using all the parameters given above in order to obtain the optical confinement factor (OCF). Then, both 3D and 2D FDTD simulations with reflectless perfectly matched layer (PML) boundary condition were carried out[16]. A non-uniform computational mesh was employed and the mesh size at the surface of metal was set to be 4 nm, which was much smaller than the expected penetration depth of plasmon field in gold (~20 nm). A waveguide optical mode was calculated as the optical source. Fig. 5 (a) and (b) showed the optical field distribution of TM waveguide

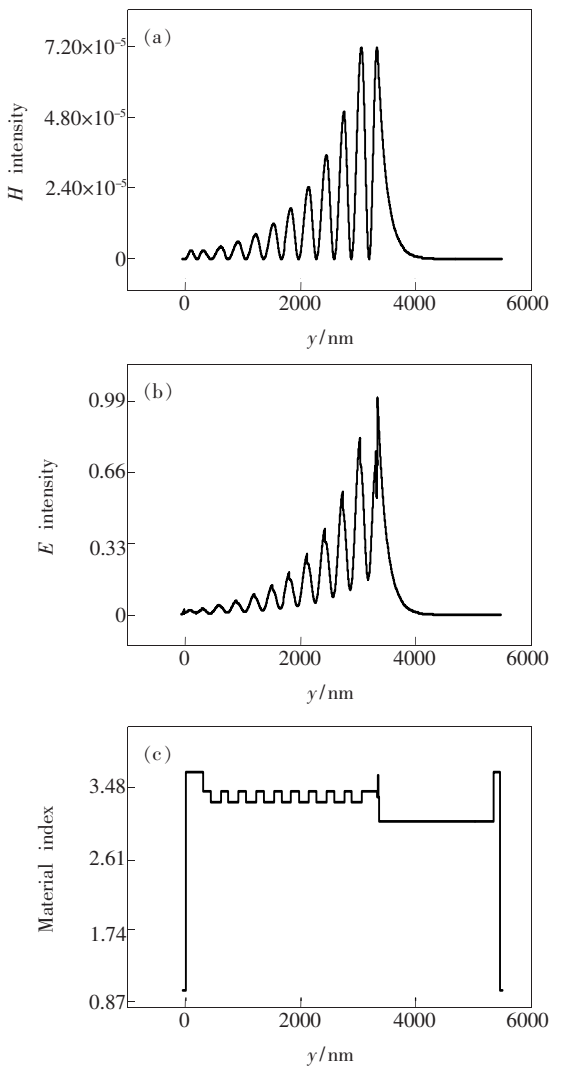

Fig. 5 Optical mode in the designed semiconductor cavity. (a) H intensity of the optical mode along the y axis. (b) E intensity of the optical mode along y axis. (c) Refractive index in the semiconductor part along y axis.

optical mode. Fig. 5(c) showed the material index profile in the semiconductor part along z axis. The effective index of this mode was calculated to be 3.089. Fig. 5 revealed that, the electric field distribution of the waveguide optical mode had an attenuated dispersion in the BRW but reduced quickly in the TIR waveguide, justed as we had expected. Fig. 6 showed the calculated near field pattern in the BRW ridge. We get the OCF $\Gamma \sim 1.245\%$, which was defined as the percentage of electrical power in the active region (11 nm $GaAs_{0.86}P_{0.14}$ QW) to total electrical power in the waveguide[17].

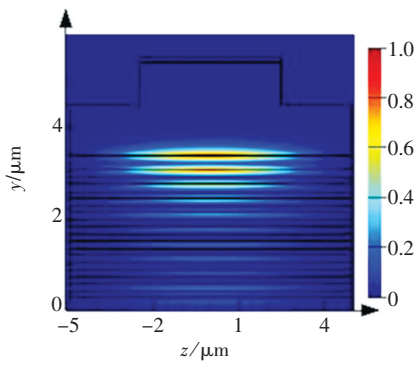

Fig. 6　The calculated optical mode field for TM_{00} mode

Condering the loss, both internal loss and mirror loss were taken into account. The influence of inducing the plasmonic region was treated as the influence on the reflectivity of one facet, which was counted into the mirror loss part. The possible scattering loss induced by the roughness side-wall was ignored. The absorption losses due to the doping level in the semiconductor part were considered. Suppose the loss is 7 cm^{-1} per 10^{18} cm^{-3} doping concentration for holes and 5 cm^{-1} per 10^{18} cm^{-3} doping concentration for electrons[18-19]. The doping concentrations of n-doped and p-doped layers on each side of the QW were assumed to be 1×10^{18} cm^{-3} and 5×10^{17} cm^{-3}, respectively. P^+ doped and n^+ layers were not considered, since very little power of the optical mode was distributed there according to Fig. 6. The material loss and refractive index $n - ik$ obey $\alpha = 4\pi k/\lambda$. Taking all these into account, α_i was calculated as 3.81 cm^{-1} in our optical mode numerical simulation.

According to Ref. [17], the material threshold gain and the photon lifetime τ_p are defined as:

$$g_{th} = \alpha_i + \frac{1}{L}\ln\frac{1}{\sqrt{R_1 R_2}}, \tag{7}$$

and

$$\tau_p = \frac{n_{eff}}{c g_{th}}, \tag{8}$$

where c is the light speed in vacuum, α_i is the internal loss, L is the laser cavity length, R_1 and R_2 are the reflectivity of the two facets.

Suppose the other facet without SiO_2 and gold has a reflectivity of $R_1 = 99.5\%$ by coating high reflection layers. A 3D FDTD has been carried out to evaluate the reflection on this specific quasi-Otto configuration facet, by varying the thickness of SiO_2 from 300 nm to 3 000 nm. Fig. 7 gave the relationship between the power going $+y$, $-y$, R_2 and metal loss. Fig. 8 showed the relationship of threshold and photon life in the semiconductor cavity *vs.* the thickness of SiO_2. Fig. 9 showed the electrical intensity along x-y facet intersection at $z = 0$. When the

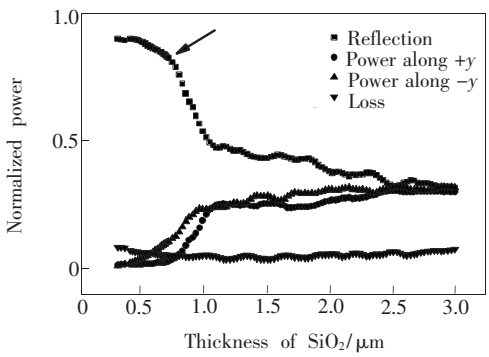

Fig. 7　Relationship between power going $+y$, $-y$, reflection at the quasi-Otto configuration facet (R_2) and metal loss simulated by 3D FDTD method.

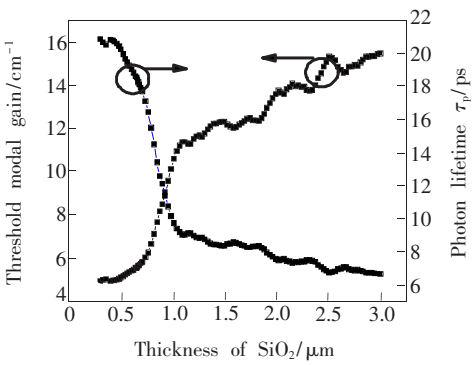

Fig. 8　Threshold modal gain and the photon lifetime τ_p at the quasi-Otto configuration facet (R_2) *vs.* thickness of SiO_2

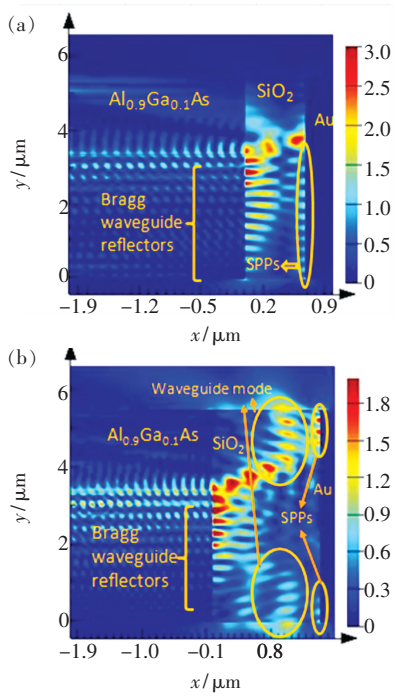

Fig. 9 The electrical intensity along x-y facet intersection at $z = 0$. (a) SiO_2 thickness of 700 nm. (b) SiO_2 thickness of 1 500 nm.

thickness of SiO_2 increased from 300 nm to around 700 nm, the reflection dropped slowly but the total power going along $+y$ and $-y$ increased. This was because when the size increased, the hybrid mode caused by semiconductor-SiO_2-metal gradually decoupled into SiO_2-metal mode— the standard SPP mode. Thus more photons met the coupling condition and coupled into SPPs, so the output power increased meanwhile the reflection reduced. The power coupled into SPPs along $+y$ was very little, only 2.4% comparing to 10% along $-y$ at 700 nm for SiO_2 thickness, where we had a threshold modal gain of 5.79 cm^{-1}. For the tensile strain single $GaAs_{0.86}P_{0.14}/Al_{0.6}Ga_{0.4}As$ QW, the peak material gain of 2 000 ~ 3 000 cm^{-1} has been demonstrated[20-21]. Consider the OCF Γ was 1.245% given above, so the population inversion for this designed BRW plasmonic laser was possible to be less than 0.2, which means the low threshold current and RT operation. When gain met loss and the current was above the threshold, our source would have begun to laser out SPPs. If only the semiconductor part had an output power more than 10 mW, which is quite normal for edge emitting semiconductor components, the total output SPP power would have reached over mill watt correspondingly.

When the thickness of SiO_2 increased more than about 700 nm, a waveguide mode in SiO_2 caused by the interference from photons reflect off metal and the photons incident toward the metal began to emerge. Different from standard Otto configuration, this mode appeared because waveguide optical mode source, instead of plane wave source, is used for optical source. This was a low loss mode. Thanks to this low loss mode, the reflection began to drop rapidly and output power began to increase along both $+y$ and $-y$ axis. However, this was no longer purely SPP mode anymore. We could see clearly a waveguide mode pattern (left peak) and a SPP mode pattern (right peak) at the SiO_2 thickness 1 500 nm. This waveguide mode could also find its applications in detection and fiber coupling. Hence, the optimized SiO_2 thickness for the SPPs emission is 700 nm according to above discussion.

Furthermore, we could see that the threshold went up and reflection went down as the thickness of SiO_2 increased. Yet they finally reach their limit at about 3 000 nm, because the coupling from photons to SPPs would not increase when the size of SiO_2 were getting too large, meanwhile the waveguide mode in SiO_2 stayed stable as the size of SiO_2 increased. The corresponding threshold modal gain maintained at about 15.44 cm^{-1}, power going $+y$, $-y$ and the reflection reached about 31%.

5 Conclusion

A new type of plasmonic laser source based on Bragg waveguide reflectors, instead of plasmonic nano-cavity has been desinged and analyzed. The optimized thickness of the dielectric material is analized and determined to be 700 nm for the emission of SPPs mode. A corresponding output plasmonic energy is 2.4% of the optical mode source along $+y$, and 10% of the optical mode source along $-y$. The threshold mode gain is 5.79 cm^{-1}. Since this structure is built on the facet of a Bragg reflection waveguide semiconductor laser, and the threshold mode gain is quite low, we believe it can work

under RT. If only the optical mode source can reach 10 mW, the output plasmonic power possilly reaches over milliwatt scale. This kind of laser can find its applications in mutiple fields such as sensing, nano-lithography and data recording meanwhile easy for integration on optical circuits.

References:

[1] Oulton R F, Sorger V J, Genov D A, *et al.* A hybrid plasmonic waveguide for subwavelength confinement and long-range propagation [J]. *Nat. Photon.*, 2008, 2(8):495-500.

[2] Oulton R F, Sorger V J, Zentgraf T, *et al.* Plasmon lasers at deep subwavelength scale [J]. *Nature*, 2009, 461(7246): 629-632.

[3] Noginov M A, Zhu G, Belgrave A M, *et al.* Demonstration of a spaser-based nanolaser [J]. *Nature*, 2009, 460(7259): 1110-1112.

[4] Ma R M, Oulton R F, Sorger V J, *et al.* Room-temperature sub-diffraction-limited plasmon laser by total internal reflection [J]. *Nat. Mater.*, 2010, 10(2):110-113.

[5] Stipe B C, Strand T C, Poon C C, *et al.* Magnetic recording at 1.5 Pb m^{-2} using an integrated plasmonic antenna [J]. *Nat. Photon.*, 2010, 4(7):484-488.

[6] Han J, Fan Y C, Zhang Z R. Propagation of surface plasmon polaritons in a ring resonator with PT-symmetry [J]. *Chin. J. Lumin.* (发光学报), 2012, 33(8):901-904 (in Chinese).

[7] Yang Z L, Fang W, Yang Y Q. Two-photon-excited fluorescence enhancement caused by surface plasmon enhanced exciting light [J]. *Chin. J. Lumin.* (发光学报), 2013, 34(2):240-244 (in Chinese).

[8] Zheng L, Zhao Y P. Identification of Pu'er teas with different fermentation time by surface-enhanced Raman scattering technology [J]. *Chin. J. Lumin.* (发光学报), 2013, 34(2):230-234 (in Chinese).

[9] Anker J N, Hall W P, Lyandres O, *et al.* Biosensing with plasmonic nanosensors [J]. *Nat. Mater.*, 2008, 7(6): 442-453.

[10] Dionne J A, Diest K, Sweatlock L, *et al.* Plasmostor: A metal-oxide-Si field effect plasmonic modulator [J]. *Nano Lett.*, 2009, 9(2):897-902.

[11] Zijlstra P, Chon J W M, Gu M. Five-dimensional optical recording mediated by surface plasmons in gold nanorods [J]. *Nature*, 2009, 459(7245):410-413.

[12] Otto A. New method for exciting non-radioactive surface plasma oscillations [J]. *Phys. Stat. Sol.*, 1968, 26:K99-K101.

[13] Otto A. Excitation of nonradiative surface plasma waves in silver by the method of frustrated total reflection [J]. *Zeitschrift für Physik*, 1968, 216(4):398-410.

[14] Kretschmann E, Reather H. Radiative decay of nonradiative surface plasmon excited by light [J]. *Z. Naturf.*, 1968, 23A:2135-2136.

[15] Maier S A. *Plasmonics: Fundamentals and Applications* [M]. United Kingdom: Springer, 2007:21.

[16] Taflove A, Hagness S C. *Computational Electrodynamics: The Finite-Difference Time-Domain Method* [M]. New York: Artech House, 2005.

[17] Coldren L A, Corzine S W. *Diode Lasers and Photonic Integrated Circuits* [M]. New York: John-Wiley, 1995.

[18] Manolatou C, Rana F. Nanoscale surface-emitting semiconductor plasmon lasers [J]. *SPIE*, 2008, 7033:70331P-1-12.

[19] Babic D I, Piprek J, Streubel K, *et al.* Design and analysis of double- fused 1.55-μm vertical-cavity Lasers [J]. *IEEE J. Quant. Elect.*, 1997, 33(8):1369-1383.

[20] Zhang Y, Ning Y Q, Zhang L, *et al.* Design and comparison of GaAs, GaAsP and InGaAlAs quantum-well active regions for 808-nm VCSELs [J]. *Opt. Exp.*, 2011, 19(13):12569-12581.

[21] Baliga A, Agahi F, Anderson N G, *et al.* Tensile strain and threshold currents in GaAsP-AlGaAs single-quantum-well lasers [J]. *IEEE J. Quant. Elect.*, 1996, 32(1):29-37.